



Optics Letters

Mirror-rotation-symmetrical single-focus spiral zone plates

ZHEN-NAN TIAN,¹  QI-DAI CHEN,^{1,4} ZHI-YONG HU,¹ YI-KE SUN,³ YAN-HAO YU,¹ HONG XIA,¹
AND HONG-BO SUN^{1,2,5}

¹State Key Laboratory of Integrated Optoelectronics, College of Electronic Science and Engineering, Jilin University, Changchun 130012, China

²State Key Laboratory of Precision Measurement Technology and Instruments, Department of Precision Instrument, Tsinghua University, Haidian, Beijing 100084, China

³School of Physical Sciences, University of Science and Technology of China, Hefei, Anhui 230026, China

⁴e-mail: chenqd@jlu.edu.cn

⁵e-mail: hbsun@tsinghua.edu.cn

Received 30 April 2018; revised 23 May 2018; accepted 23 May 2018; posted 31 May 2018 (Doc. ID 330102); published 25 June 2018

In this Letter, we report mirror-rotation-symmetrical single-focus spiral zone plates (MS-SZPs) fabricated by femtosecond laser direct writing. The novel optical element can generate a single-focus vortex beam, owing to the element's complicated continuous surface. The MS-SZP surface possesses reverse mirror-rotation symmetry, which ensures that the transfer element has the same surface morphology as the original element. Both the transfer element and original element have good optical properties. The single-focus behavior was investigated by a microscopic imaging system and found to be in good agreement with theoretical simulation results. The innovative optical component is expected to be widely used in optical communication, quantum computation, optical manipulation, and other fields. © 2018 Optical Society of America

OCIS codes: (230.3990) Micro-optical devices; (220.0220) Optical design and fabrication; (140.7090) Ultrafast lasers; (220.4000) Microstructure fabrication.

<https://doi.org/10.1364/OL.43.003116>

The optical vortex (OV) has attracted great interest for its unique and fascinating properties, which differ from those of traditional light beams, since its discovery by Allen *et al.* in 1992 [1–4]. OV beams possess a helical phase front and intrinsic orbital angular momentum (OAM), giving them potential for applications in terabit-level data transmission [5], multidimensional coding in quantum calculation, and optical manipulation [6,7]. In recent decades, various interesting methods based on different optical theories have been proposed to generate OV beams, such as geometric methods, spiral phase plates (SPPs), spiral zone plates (SZPs), spatial light modulators, *Q*-plates, metasurfaces, and hybrid optical elements [8–12]. These typical methods have contributed considerably to broadening the applications of OV beams.

SZPs, which are a variation on the Fresnel zone plate (FZP) and SPP, were proposed by Heckenberg *et al.* as a simple OV

beam generator [13]. The FZP and SPP focus and generate a helical wave front, respectively. However, the conventional FZP is a binary diffraction element; in addition to the first-order focus at f needed for their design, the FZP has extra multiple high-order foci at $f/3$, $f/5$, $f/7$, and so on [14]. The undesired high-order foci not only reduce the diffraction efficiency, but also increase the background noise, which seriously affects the optical properties of optical components. Many methods have been proposed to solve this problem, such as a subwavelength structure, multilevel structure, and gray transmittance elements [15,16]. Another well-known strategy, the Gabor zone plate (GZP), was proposed in the 1950s [17]. This special zone plate can effectively suppress the occurrence of orders higher than the first order. However, because it is limited by the processing capacity, the zone plate was not realized for a long time. After nearly 40 years, reports on the fabrication of GZPs began to appear and gradually attracted researchers' attention. In 2017, Xie's group proposed a single-focus SZP based on the GZP, which is a simple and compact optical element [14]. The element shows good optical properties and is well-suited to fabrication by modern lithography technology. However, all of the existing components based on the GZP work as amplitude modulator elements, which change the amplitude of light waves by blocking some regions of the elements.

Here, we present continuous-surface SZPs (MS-SZPs) based on GZPs. The novel element can generate a single-focus OV beam, benefiting from the continuous light modulation by the elements' complicated surface. The surface of the element resembles a spiral water wave overall, and its profile is a cosine curve with decreasing periodicity. The complex surface is difficult to process by traditional machining techniques. Two-photon photopolymerization induced by femtosecond laser direct writing (FsLDW), which has been widely used in high-precision three-dimensional machining of arbitrary structures, can acceptably solve this problem [18–22]. The geometrical structure of the element is in perfect agreement with the theoretical design, which ensures that the element possesses the expected fine optical performance. Furthermore, the element has reverse mirror-rotation symmetry, which means that the transfer element has

the same surface profile as the original element. Both the transfer element and original element have good optical properties.

The continuous-phase single-focus MS-SZP is a combination of an SPP and GZP, whose transmittance functions can be written as

$$T_{\text{SPP}}(r, \theta) = A * \exp(i * P * \theta), \quad (1)$$

$$T_{\text{GZP}}(r, \theta) = A * \exp(i * 2\pi r^2 / 2\lambda f), \quad (2)$$

where r and θ are polar coordinates, and P represents the topological charge. Further, λ and f are the designed wavelength and focal length of the GZP, respectively. For a pure phase-type optical element, the amplitude A is equal to one, which means that all the light is transmitted without loss. The transmittance function of the MS-SZP can be obtained by multiplying Eqs. (1) and (2):

$$T_{\text{MS-SZP}}(r, \theta) = T_{\text{SPP}}(r, \theta) * T_{\text{GZP}}(r, \theta). \quad (3)$$

The modulated amplitude distributions of Eqs. (1)–(3) are shown in Figs. 1(a)–1(c), respectively. To show the functions more clearly, they were multiplied by an aperture function and normalized. A transmittance function image of an SPP with a topological number of one is shown in Fig. 1(a). Around the center of the structure, the height gradually increases from 0° to 360° along the angular direction and then decreases rapidly to the minimum height at 360°. Figure 1(b) shows a function image of Eq. (2). Along the radial direction, the profile of the structure is a cosine curve with a gradually decreasing period. Figure 1(c) shows a transmittance function image of a MS-SZP with a topological number of one, which has a more complex surface morphology. The structure has reverse mirror-rotation symmetry, and it will be realized by FsLDW technology.

The MS-SZP was fabricated using FsLDW technology based on two-photon polymerization. As a well-known microprocessing technology, FsLDW has been widely used to produce micro-optical elements, micromechanical structures, and microfluidic chips owing to its unique, high-precision, and real three-dimensional processing capability [23–27]. In the experiment, a fiber femtosecond laser (LF7808, Shanghai Langyan Optoelectronics Technology Co. Ltd.) was used; its wavelength, pulse width, and repetition rate are 780 nm, 100 fs, and 80 MHz, respectively. When a mature femtosecond laser processing system is used, the laser focus can provide point-by-point scanning of a material. Here, a commercial negative photoresist, SU-8 (2025, MicroChem Corp.), with high transmittance and good mechanical properties was used. After pre-baking, laser scanning, post-baking, and development, the MS-SZPs are obtained, as shown in Fig. 2. The 45° tiled views of MS-SZPs with topological numbers of one, two, and three were taken by laser confocal microscopy (LSCM, OLS3000,

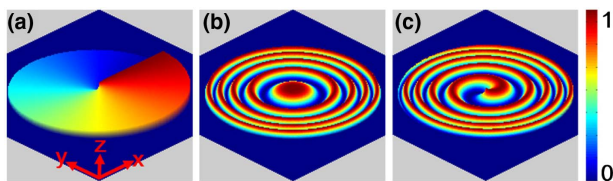


Fig. 1. Normalized transmittance function distribution of (a) SPP, (b) GZP, and (c) MS-SZP, which correspond to Eqs. (1)–(3), respectively. All of the equations were multiplied by an aperture function and normalized.

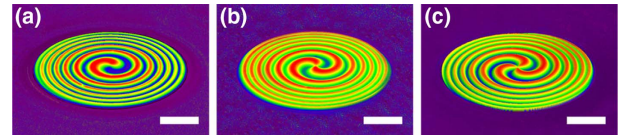


Fig. 2. Laser confocal microscopy images (45° tiled view) of MS-SZPs with topological numbers of (a) one, (b) two, and (c) three. Scale bar: 10 μm .

EVC electronic). The diameter, height, and focal length of the MS-SZPs shown in Fig. 2 are 80 μm , 1.1 μm , and 100 μm , respectively. The surface of the element is continuous without any obvious abrupt changes (i.e., step structure). Overall, the geometric morphology of the elements was in good agreement with the design.

The profile of the MS-SZP is a cosine curve with gradually decreasing periodicity. For an element with topological number P , it has a $2\pi/P$ degree reverse mirror-rotation symmetry, which means that the transfer element has the same geometric morphology as the original element used in the transfer process. Figure 3 shows images of the original MS-SZPs and transfer MS-SZPs taken by scanning electron microscopy (SEM, JSM-7500F, JEOL). Figures 3(a)–3(c) show the original MS-SZPs with topological numbers of one, two, and three, which were used as templates and sealed with a layer of polydimethylsiloxane (PDMS, Sylgard 184, Dow Corning) prepolymer. The template element and PDMS prepolymer were warmed in a conventional drying oven at 60°C for 6 h. After the prepolymer was peeled off, the transfer MS-SZPs were obtained, as shown in Figs. 3(d)–3(f). The transfer element has the exact same surface profile as the original template. However, owing to the reverse mirror symmetry of MS-SZPs, the helical structure of the transfer elements has the opposite rotation extension direction from that of the original elements.

To more clearly and quantitatively characterize the geometric morphology of the MS-SZPs, the theoretical and experimental profiles are shown in Fig. 4. Figures 4(a) and 4(b) show the profiles of the original element and transfer element, respectively. The MS-SZP with a topological number of one

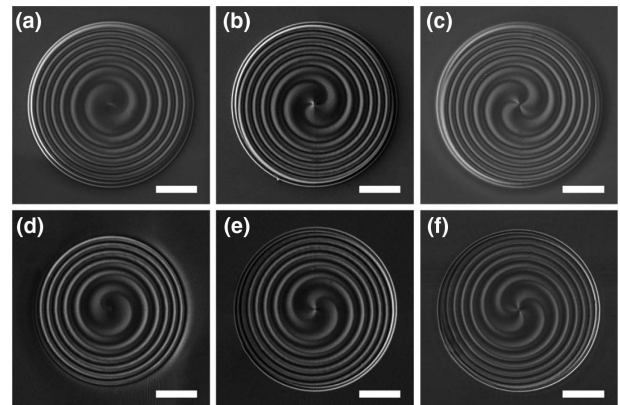


Fig. 3. SEM images of the (a)–(c) original MS-SZPs and (d)–(f) transfer MS-SZPs. MS-SZPs with topological numbers of one, two, and three were used. Notice that, except for the opposite rotation direction, the transfer element and original element have exactly the same surface. Scale bar: 10 μm .

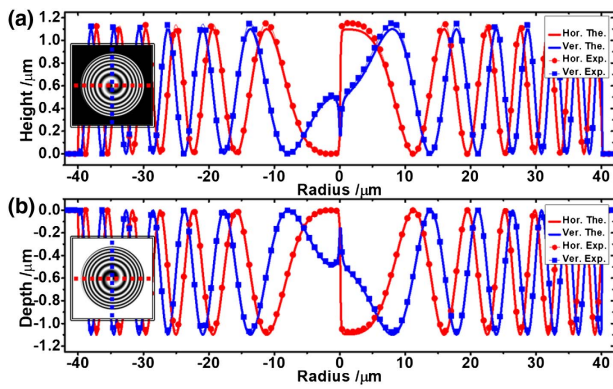


Fig. 4. Surface profile of (a) original MS-SZPs and (b) transfer MS-SZPs. The solid and dotted lines are the theoretical design and experimental measurement results, respectively. The inset indicates the position relationship between the profile figure and element. Note the difference of the scale in the lateral axes. The height variation of the original element and transfer element is complementary.

was used. The red and blue lines show the surface undulations in the horizontal and vertical directions, respectively. The relative positions of the profile and element are shown in the inset by red and blue dotted lines, respectively. The solid lines and dotted lines represent the theoretical design and experimental measurement results, respectively. The variation in height with the radius of the transfer element is complementary to that of the original element. The surface profiles of both the original element and the transfer element are clearly consistent with the theoretical design. The maximum error between the experiment and theory is less than 2%, which ensures that the elements possess desirable optical characteristics.

The MS-SZPs can generate an OV beam carrying an OAM. Unlike the spin angular momentum (SAM), which has only two values, $\pm\hbar$, per photon, an OV beam can carry an intrinsic OAM of $\pm l\hbar$ per photon. In principle, the topological charge l can be an arbitrary positive or negative integer. The unlimited states of the OAM enable it to carry more signals in both classical and quantum communication systems. The OV beam possesses a helical wavefront and phase singularity; consequently, its focus energy distribution is a hollow ring rather than solid. The size of the hollow ring varies with the topological charge of the OV beam. Figure 5 shows the relationship between the topological charge and light size. The original and transfer MS-SZPs with topological charges of one, two, and three were used; their diameter and focal length were 80 μm and 100 μm , respectively, as shown in Fig. 3. An expanded He–Ne laser with a wavelength of 633 nm was used as a light source to irradiate the element vertically. Behind the element, the energy distribution of the light spot was observed by an imaging system composed of an objective lens and a complementary metal–oxide–semiconductor (CMOS) image sensor. The light spot diameters of the original MS-SZPs with topological numbers of one, two, and three were 1.26, 2.24, and 2.85 μm , as shown in Figs. 5(a)–5(c), respectively. The diameters of the corresponding transfer elements were 1.3, 2.4, and 2.96 μm , as shown in Figs. 5(d)–5(f). The focal spots of the corresponding elements have essentially the same size, owing to the reverse mirror-rotation symmetry of the element

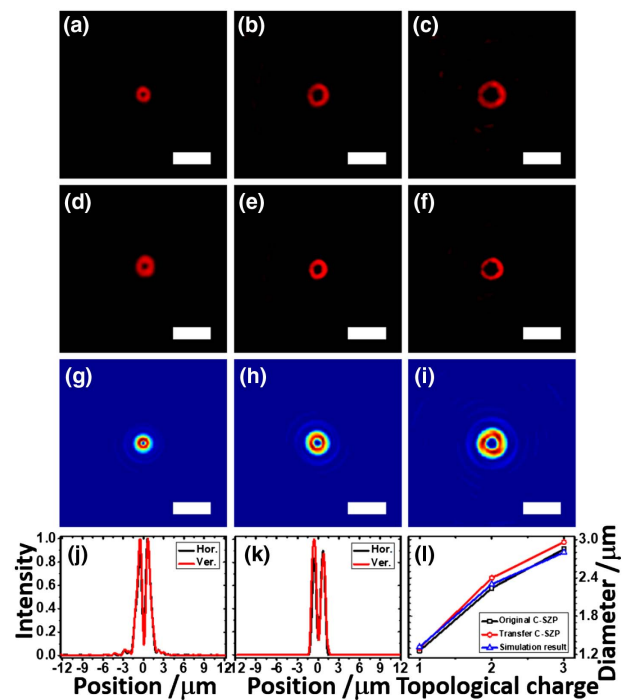


Fig. 5. Focused light spot of MS-SZPs with topological numbers of one, two, and three. (a)–(c) Original element, (d)–(f) transfer element, and (g)–(i) simulation results. Normalized energy distribution in the cross section of the focal spot from the (j) simulation and (k) experiment. (l) Relationship between light spot size and topological number in experiment and simulation.

itself and the geometric agreement after transfer. The corresponding theoretical simulation results are 1.32, 2.3, and 2.8 μm , as shown in Figs. 5(g)–5(i). In the simulation, a Gaussian light beam was used as a light source. The normalized energy distribution in the cross section of the focal spot in the simulation and experiment are shown in Figs. 5(j) and 5(k), where the light spots in Figs. 5(a) and 5(g) are used, respectively. The black and red lines represent the energy distributions of the light spot in the horizontal and vertical directions, respectively. The size of the light spot and energy distribution in the experiment and simulation show no obvious difference. The spot size increased gradually with the increasing topological number in both the experiment and the simulation, as shown in Fig. 5(l).

The most important property of the MS-SZP is that it has only one focal point along the optical axis, owing to its complex continuous-surface design. This significant single-focus characteristic was investigated in the experiment and simulation, as shown in Fig. 6. By changing the position of the energy observation imaging system, the distribution of the light energy at different positions behind the element can be investigated. Figures 6(a)–6(d) show the light intensity at 100, 33, 20, and 14 μm , which correspond to f , $f/3$, $f/5$, and $f/7$, respectively. The theoretical simulation results are shown in Figs. 6(e)–6(h). Unlike the case of traditional optical elements, which would focus light at the above positions, there is no obvious multifocus phenomenon behind the MS-SZPs in either the experiment or the simulation. To more clearly demonstrate the single-focus behavior, the energy distribution along the

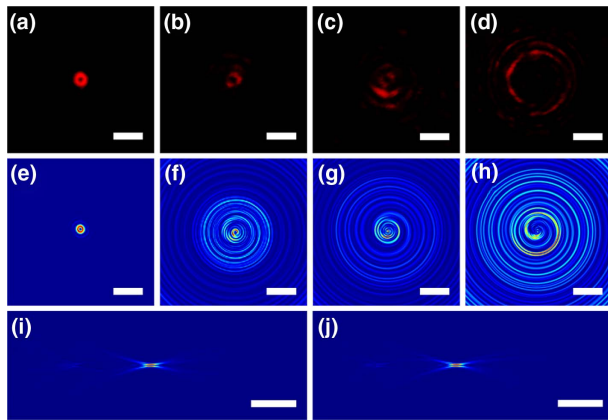


Fig. 6. Energy distributions at different positions behind the MS-SZPs. Experimental results: (a) f , (b) $f/3$, (c) $f/5$, (d) $f/7$. Simulation results: (e) f , (f) $f/3$, (g) $f/5$, (h) $f/7$. (i), (j) Intensity distribution along the optical axis. Scale bar: (a)–(h) 10 μm ; (i), (j) 30 μm .

optical axis was calculated. The calculated light intensities within 200 μm behind the element in the horizontal and vertical directions are shown in Figs. 6(i) and 6(j), respectively. It is very obvious that there is only one focus area near 100 μm from the element, where the spatial distribution of the energy is cylindrical.

In summary, we report a novel OV beam generator called the MS-SZP, which is a combination of an SPP and a GZP. Its surface is continuous without abrupt steps, which possesses reverse mirror-rotation symmetry. The OV generated by the MS-SZP has only one focus, so the beam quality is not degraded by multifocal scattered light. The single-focus behavior was investigated experimentally and was found to be in good agreement with the results of a theoretical simulation. Owing to the mirror-rotation symmetry, the transfer element has the same surface morphology as the original element, suggesting that mass reproduction of the MS-SZP is possible. The MS-SZP design method is universally available, opening a new avenue to realizing high-performance single-focus mirror symmetry elements.

Funding. National Key Research and Development Program of China; National Natural Science Foundation of China (NSFC) (2017YFB1104600, 2014CB921302, 61590930, 61435005, 51335008).

REFERENCES

1. L. Allen, M. W. Beijersbergen, R. J. C. Spreeuw, and J. P. Woerdman, *Phys. Rev. A* **45**, 8185 (1992).
2. D. G. Grier, *Nature* **424**, 810 (2003).
3. S. J. Zhang, Y. Li, Z. P. Liu, J. L. Ren, Y. F. Xiao, H. Yang, and Q. H. Gong, *Appl. Phys. Lett.* **105**, 061101 (2014).
4. E. Brasselet, M. Malinauskas, A. Zukauskas, and S. Juodkazis, *Appl. Phys. Lett.* **97**, 211108 (2010).
5. T. Lei, M. Zhang, Y. R. Li, P. Jia, G. N. Liu, X. G. Xu, Z. H. Li, C. J. Min, J. Lin, C. Y. Yu, H. B. Niu, and X. C. Yuan, *Light Sci. Appl.* **4**, e257 (2015).
6. X. L. Wang, J. Chen, Y. N. Li, J. P. Ding, C. S. Guo, and H. T. Wang, *Phys. Rev. Lett.* **105**, 253602 (2010).
7. J. Leach, B. Jack, J. Romero, A. K. Jha, A. M. Yao, S. Franke-Arnold, D. G. Ireland, R. W. Boyd, S. M. Barnett, and M. J. Padgett, *Science* **329**, 662 (2010).
8. X. W. Wang, A. A. Kuchmizhak, E. Brasselet, and S. Juodkazis, *Appl. Phys. Lett.* **110**, 181101 (2017).
9. Y. Pan, X. Z. Gao, Z. C. Ren, X. L. Wang, C. H. Tu, Y. N. Li, and H. T. Wang, *Sci. Rep.* **6**, 29212 (2016).
10. M. Malinauskas, A. Zukauskas, S. Hasegawa, Y. Hayasaki, V. Mizeikis, R. Buividas, and S. Juodkazis, *Light Sci. Appl.* **5**, e16133 (2016).
11. M. Gecevicius, M. Ivanov, M. Beresna, A. Matijosius, V. Tamuliene, T. Gertus, A. Cerkauskaitė, K. Redeckas, M. Vengris, V. Smilgevičius, and P. G. Kazansky, *J. Opt. Soc. Am. B* **35**, 190 (2018).
12. A. Žukauskas, M. Malinauskas, and E. Brasselet, *Appl. Phys. Lett.* **103**, 181122 (2013).
13. Z. N. Tian, J. G. Hua, J. Hao, Y. H. Yu, Q. D. Chen, and H. B. Sun, *Appl. Phys. Lett.* **110**, 041102 (2017).
14. Y. H. Liang, E. L. Wang, Y. L. Hua, C. Q. Xie, and T. C. Ye, *Opt. Lett.* **42**, 2663 (2017).
15. Z. Cai, Y. Liu, C. C. Zhang, J. C. Xu, S. Y. Ji, J. C. Ni, J. W. Li, Y. L. Hu, D. Wu, and J. R. Chu, *Opt. Lett.* **42**, 2483 (2017).
16. H. Guan, H. Chen, J. Wu, Y. Jin, F. Kong, S. Liu, K. Yi, and J. Shao, *Opt. Lett.* **39**, 170 (2014).
17. G. L. Rogers, *Nature* **166**, 237 (1950).
18. L. Wang, Q. D. Chen, X. W. Cao, R. Buividas, X. W. Wang, S. Juodkazis, and H. B. Sun, *Light Sci. Appl.* **6**, e17112 (2017).
19. X. Q. Liu, Q. D. Chen, K. M. Guan, Z. C. Ma, Y. H. Yu, Q. K. Li, Z. N. Tian, and H. B. Sun, *Laser Photon. Rev.* **11**, 1600115 (2017).
20. K. Sugioka and Y. Cheng, *Light Sci. Appl.* **3**, e149 (2014).
21. Z. F. Deng, Q. Yang, F. Chen, X. W. Meng, H. Bian, J. L. Yong, C. Shan, and X. Hou, *Opt. Lett.* **40**, 1928 (2015).
22. H. B. Jiang, Y. L. Zhang, Y. Liu, X. Y. Fu, Y. F. Li, Y. Q. Liu, C. H. Li, and H. B. Sun, *Laser Photon. Rev.* **10**, 441 (2016).
23. Z. Zhang, Y. H. Zhang, H. Fan, Y. L. Wang, C. Zhou, F. F. Ren, S. Z. Wu, G. Q. Li, Y. L. Hu, J. W. Li, D. Wu, and J. R. Chu, *Nanoscale* **9**, 15796 (2017).
24. Y. L. Sun, Q. Li, S. M. Sun, J. C. Huang, B. Y. Zheng, Q. D. Chen, Z. Z. Shao, and H. B. Sun, *Nat. Commun.* **6**, 8612 (2015).
25. Z. H. Wang, B. Zeng, G. H. Li, H. Q. Xie, W. Chu, F. He, Y. Liao, W. W. Liu, H. Gao, and Y. Cheng, *Opt. Lett.* **40**, 5726 (2015).
26. F. Chen and J. R. V. de Aldana, *Laser Photon. Rev.* **8**, 251 (2014).
27. J. C. Ni, C. W. Wang, C. C. Zhang, Y. L. Hu, L. Yang, Z. X. Lao, B. Xu, J. W. Li, D. Wu, and J. R. Chu, *Light Sci. Appl.* **6**, e17011 (2017).